Resilient Operation of Electric Power Distribution Grids Under Progressive Wildfires

Mostafa Nazemi, *Student Member, IEEE*, Payman Dehghanian, *Senior Member, IEEE*, Mohannad Alhazmi, *Student Member, IEEE*, and Yousef Darestani

***Abstract*—Wildfires have been growingly recognized as a prominent threat in regions with high temperatures during the summer. Power distribution systems, especially those passing through forest regions, are exposed and highly vulnerable to wildfires. This article provides a general formulation to enhance the operational resilience of power distribution networks equipped with renewable energy resources, e.g., wind and solar energy, micro turbines as well as energy storage systems when exposed to progressive wildfires. The wildfire incident is characterized comprehensively and the dynamic heat balance equations of power distribution branches are used to model the impacts of wildfires on overhead line conductors. A mixed-integer quadratic optimization formulation is applied to optimally operate and coordinate all local energy resources to reduce load outages and enhance the system resilience. The applied framework is evaluated on the IEEE 33-node test system. Comprehensive sensitivity analyses are conducted to assess the efficacy of the applied framework, where the numerical results reveal the resilient operation of power distribution networks in the face of wildfire emergencies.**

***Index Terms*—Distributed energy resources, power distribution systems, resilience, wildfire hazards,.**

Nomenclature

A. Abbreviations

DHB	Dynamic heat balance
ESSs	Energy storage systems
RESs	Renewable energy resources
MTs	Micro-turbines
PV	Photovoltaic energy
WT	Wind turbine
SoC	State of charge

B. Sets and Indices

$i, j \in \mathbf{B}$	Indices/set of nodes.
$j \in \mathbf{B_i}$	Set of nodes adjacent to node i.
$ij \in \mathbf{L}$	Indices/set of distribution lines between nodes i and j.
$ij \in \ell$	Indices/set of power distribution lines between nodes i and j affected by wildfire.
$t \in \mathbf{T}$	Indices/set of time periods.
$\omega \in \mathbf{\Omega}$	Indices/set of scenarios.

C. Parameters and Constants

1) Fire Parameters

T^f	Flame zone temperature (K).
ν^f	Fire front length (m).
α^f	Fire tilt angle (rad).
ρ^b	The bulk density of the fuel $(\mathrm{kg/m^3})$.
ε^f	Flame zone emissivity.

2) Environmental Conditions

τ	Dimensionless atmospheric transmissivity.
B	Stefan–Boltzman constant $(\mathrm{W/m^2}K^4)$.
V^{wind}	Wind speed (m/s).
σ^{wind}	Angle between the wind direction and conductor axis (rad).
T^a	Ambient temperature (K).
k^a	Thermal conductivity of air $(\mathrm{W/m}K)$.
μ^α	Air dynamic viscosity (kg/ms).
ρ^α	Air density $(\mathrm{kg/m^3})$.
K^0	Shape index of the Weibull distribution.
C	Scale index of the Weibull distribution.

3) Conductor Specifications

mC_p	Total heat capacity of conductor (J/mK).
D	Conductor diameter (m).

Manuscript received July 31, 2021; revised November 8, 2021; accepted December 10, 2021. Date of publication January 25, 2022; date of current version March 20, 2022. This work was supported by the US National Science Foundation (NSF) under Grants ICER-2022505 and ECCS-2114100. Paper 2021-PSEC-0883.R1, presented at the 2021 IEEE Industry Applications Society Annual Meeting, Vancouver, BC Canada, Oct. 10–14, and approved for publication in the IEEE Transactions on Industry Applications by the Power Systems Engineering Committee of the IEEE Industry Application Society. *(Corresponding author: Payman Dehghanian.)*

Mostafa Nazemi and Payman Dehghanian are with the Department of Electrical and Computer Engineering, George Washington University, Washington, DC 20052 USA (e-mail: mostafa_nazemi@gwu.edu; payman@gwu.edu).

Mohannad Alhazmi is with the Department of Electrical and Computer Engineering, George Washington University, Washington, DC 20052 USA, and also with the Department of Electrical Engineering, College of Engineering, King Saud University, Riyadh 11421, Saudi Arabia (e-mail: alhazmi@gwu.edu).

Yousef Darestani is with the Department of Civil and Environmental Engineering, Michigan Technological University, Houghton, MI 49931 USA (e-mail: ydaresta@mtu.edu).

Color versions of one or more figures in this article are available at https://doi.org/10.1109/TIA.2022.3145780.

Digital Object Identifier 10.1109/TIA.2022.3145780

0093-9994 © 2022 IEEE. Personal use is permitted, but republication/redistribution requires IEEE permission.
See https://www.ieee.org/publications/rights/index.html for more information.

Authorized licensed use limited to: The George Washington University. Downloaded on August 05,2022 at 03:56:01 UTC from IEEE Xplore. Restrictions apply.

∂ Solar absorptivity.
ϕ^{sun} Solar radiation rate (W/m^2).
$R_{ij,a}$ Ambient line resistance.
$T^{\max}$ Maximum permitted conductor temperature (K).

4) Price and Costs

VoLL Value of lost load (\$/MWh).
c^D Selling electricity price to customers (\$/MWh).
c^{MT} MTs generation cost (\$/MW).
$c^{su/sd}$ Startup/Shutdown cost of MTs (\$).
c_t^{UP} Electricity price at time t (\$/MWh).

5) Power Distribution System Components

$P_{i,t}^{\text{demand}}$ Real power demand at node i at time t (MW).
$Q_{i,t}^{\text{demand}}$ Reactive power demand at node i at time t (MVar).
$\bar{P}_{ij,t}^{\text{fl}}, \bar{P}_{ij,t}^{\text{fl}}$ Active power capacity limit of line ij at time t (MW).
$\bar{Q}_{ij,t}^{\text{fl}}, \bar{Q}_{ij,t}^{\text{fl}}$ Reactive power capacity limit of line ij at time t (MVar).
$\underline{V_{\text{sqr}}}_i, \overline{V_{\text{sqr}}}$ Minimum and maximum square voltage of node i (kV^2).
η^{ST} Conversion efficiency of ESSs.
E^{ST} Energy capacity of ESSs (MWh).

D. Functions and Variables

1) Fire Model

$\theta_{ij,t}^f$ View angle between fire and conductor line ij at time t (rad).
$d_{ij,t}^f$ Distance between fire and line ij at time t (m).
V_t^f Fire spread rate (m/s) at time t.
$T_{ij,t}$ Conductor temperature of line ij at time t (K).
χ_t^f Radiative heat flux at time t (W/m^2).

2) Heat Gain and Loss

$q_{ij,t}^{\text{line}}$ Resistance heat gain rate of line ij at time t (W/m).
$q_{ij,t}^{\text{sun}}$ Solar heat gain rate of line ij at time t (W/m).
$q_{ij,t}^{\text{fire}}$ Fire heat gain rate of line ij at time t (W/m).
$q_{ij,t}^{\text{con}}$ Convection heat loss rate of line ij at time t (W/m).
$q_{ij,t}^{\text{rad}}$ Radiation heat loss rate of line ij at time t (W/m).

3) Power System Model

$p_{i,t}^D, q_{i,t}^D$ Real and reactive power supplied at node i at time t (MW, MVar).
$P_{ij,t}^{\text{fl}}, Q_{ij,t}^{\text{fl}}$ Real and reactive power flow on branch ij at time t (MW, MVar).
$\text{SoC}_{i,t}^{ST}$ SoC of ESS at time t.
$p_{i,t}^{\text{Ch}}, p_{i,t}^{\text{dCh}}$ Charging and discharging power of ESS at node i at time t (MW).
$q_{i,t}^{\text{ESS}}$ Reactive power of ESS at node i at time t (MVar).
$p_{i,t}^{\text{MT}}, q_{i,t}^{\text{MT}}$ Real and reactive power output of MT at node i (MW, MVar).
$[su_{i,t}^{\text{MT}}, sd_{i,t}^{\text{MT}}$ Start-up/Shut-down costs of MTs at node i at time t (\$)
$p_{i,t}^{\text{WT}}, p_{i,t}^S$ Real power output of WT and PV at node i at time t (MW).
$V_{\text{sqr}_{i,t}}$ Squared voltage magnitude at node i at time t (kV^2).
$p_{i,t}^{\text{O}}, q_{i,t}^{\text{O}}$ Real and reactive load outage at node i at time t (MW, MVar).
p_t^{UP} Active power exchange with the upstream network at time t (MW).

E. Binary Variables

$\alpha_{ij,t}$ Connection status of branch ij at time t (1 if the branch is connected, 0 otherwise).
$u_{i,t}$ Charging and discharging status of ESS at node i at time t (1 if charging, 0 otherwise).
$\kappa_{i,t}$ Status of MT at node i at time t (1 if the MT is generating, 0 otherwise).
φ_t^{UP} Buying or selling energy from/to the up stream network at time t (1 if buying, 0 otherwise).

I. Introduction

THE growing severity and duration of power outages triggered by wildfires impose an adverse impact on the operation of multiple life-line networks and results in significant financial risks. For instance, in May 2016, a wildfire was initiated in Alberta, Canada. The direct financial loss to insurance providers from the great Alberta fire was estimated at about \$3.7 billion [1]. In October 2017, a series of wildfires started to burn across the wine county of Northern California. These wildfires caused at least \$9.4 billion in insured damages and the death of 44 people [2]. In fiscal year 2017, the cost of battling blazes topped \$2.4 billion [3]. For the first time in its 110-year history, the U.S. Forest Service is spending more than 50% of its budget fighting wildfires [4]. The California Department of Forestry and Fire Protection reports that the 2018 Woolsey and Camp fires caused \$4 billion and \$11 billion in damages, respectively [5]. In addition, wildfire risks in October 2018 and 2019 forced Pacific Gas and Electric to anticipatively cut off electricity to a sizable number of end-use consumers in high-risk areas in northern California, resulting in missed opportunity costs

Authorized licensed use limited to: The George Washington University. Downloaded on August 05,2022 at 03:56:01 UTC from IEEE Xplore. Restrictions apply.

though no wildfires happened [6]. Therefore, one can notice that maintaining the nation's electric power system resilience against wildfires and ensuring a reliable, secure, and sustainable supply of electricity during such threatening events are among the top priorities for the electric power industry.

Research efforts in the literature have studied the power system's resistance to severe fire conditions. Among, the thermal rating of the at-risk power lines was dynamically adjusted in [7] to reduce the line heat gained from the fire. In order to model the effect of wildfires on overhead conductor temperature and consequently on the flowing current, reference [8] suggested a dynamic line rating mechanism for overhead lines. Reference [9] proposed a technique for quantifying the destruction caused by wildfires to electric power distribution grids. In [10] and [11], a strategy for optimal distribution system operation in the face of a huge fire is introduced, where the operating performance of microgrids and the role of demand response programs are investigated. Reference [12] examines different faults and conditions that contribute to wildfire ignition, establishing the mathematical relation between the wind speed and the fire ignition risk. A statistical characterization model is developed in [13] to demonstrate the relationship between continuous ignition of a dry fuel bed and multiple determining parameters such as wind speed, fuel moisture content, and arc length. While the models in [11]–[15] are important to understand the wildfire ignition problem, the literature still needs to explore deeply the wildfire propagation models, which impact power distribution networks in general and the overhead power distribution conductors in particular.

The wildfire impacts on power distribution lines are not limited to the actual destruction of the structures. The wooden poles would most certainly catch fire and the conductors would melt in the event of a significant wildfire, such as one in a forest. However, there are many small to moderate wildfires that pose thermal stress on overhead wires even if there is no physical damage to the system [16]. Furthermore, the pace of annealing of the conductor will be affected by a rise in its surface temperature, and its tensile strength will be reduced.

This article focuses on resilient operation of power distribution systems in the face of approaching wildfires. Our approach to system resilience enhancement in this article is through effective mitigation, response, and recovery. This article provides power system operators with a comprehensive mitigation solution approach that once a wildfire occurs, analyzes the vulnerability of overhead power distribution branches by applying the dynamic heat balance (DHB) equations. Particularly, the temperature rise of overhead power line conductors is computed by adding the heat gained by wildfire to the other sources of heat that cause temperature rise of the conductors. Once the conductor temperature surpasses the threshold, the distribution line will become out of service resulting in load outage across the network depending on the location of unavailable lines. Under such circumstances, the role of local energy resources, i.e., renewable energy resources (RESs), micro turbines (MTs), and energy storage systems (ESSs), becomes imperative as they can mitigate the load outages by fully or partially supplying the demanded loads. This calls for an optimal operation and coordination of local energy resources to mitigate the wildfire impacts on power distribution grid and, hence, boost the system resilience by reducing the load outages during such emergencies. The contributions of this article are summarized as follows.

1) Inspired by [8], a comprehensive wildfire modeling approach is applied to capture the impacts of progressive wildfires on overhead power distribution lines.
2) The DHB concept is applied to model and account for the temperature rise of the overhead power line conductors in the face of progressive wildfires.
3) An optimization framework for resilient operation and optimal coordination of local energy resources is applied to mitigate the load outages and ensure a resilient system operation during wildfire emergencies.
4) Comprehensive sensitivity analyses are presented to highlight the accuracy of the results and to evaluate the generality of the applied resilience enhancement framework.

The rest of this article is organized as follows. The big picture of the proposed framework is illustrated in Section II. Wildfire modeling is formulated in Section III, while the power system problem formulation is provided in Section IV. Numerical case study, simulation results on a modified IEEE 33-bus test system, and comprehensive sensitivity analyses are demonstrated in Section V. This article is eventually concluded in Section VI.

II. Big-Picture of the Proposed Framework

The big picture of the proposed framework for resilient operation of power distribution networks in the face of wildfire events is depicted in Fig. 1. Stochastic parameters, i.e., solar radiation, wind speed, and wind direction, are represented by different probability distribution functions to be integrated into the optimization problem as the inputs. Wildfire modeling is applied where progressive wildfires are characterized by different parameters, including fuel types, vegetation, slope, and elevation of landscapes, wind speed and directions, ambient temperature, air density and dynamic velocity as *environmental parameters*; type and diameter of conductors, solar absorptivity, solar radiation rate, total heat capacity, and ambient line resistance as *conductor parameters*; and flame zone temperature, fire front length, fire tilt angle, and flame zone emissivity as *fire parameters*. The DHB is determined per the heat gains and losses in different time periods. The temperature of an overhead power line conductor is then obtained based on the DHB equations. Once the temperature surpasses the safety threshold, the impacted lines will become out of service resulting in some load outages. To reduce the load outages and enhance the network resilience, different local energy resources, i.e., RESs, ESSs, and MTs, should be optimally and cost-efficiently operated and coordinated. Therefore, the proposed framework applies a comprehensive optimization formulation in which different types of power system operation constraints as well as those for distributed energy resources are included. Subsequently, the formulation is linearized, and then convexified to be solved by off-the-shelf optimization solvers.

Authorized licensed use limited to: The George Washington University. Downloaded on August 05,2022 at 03:56:01 UTC from IEEE Xplore. Restrictions apply.

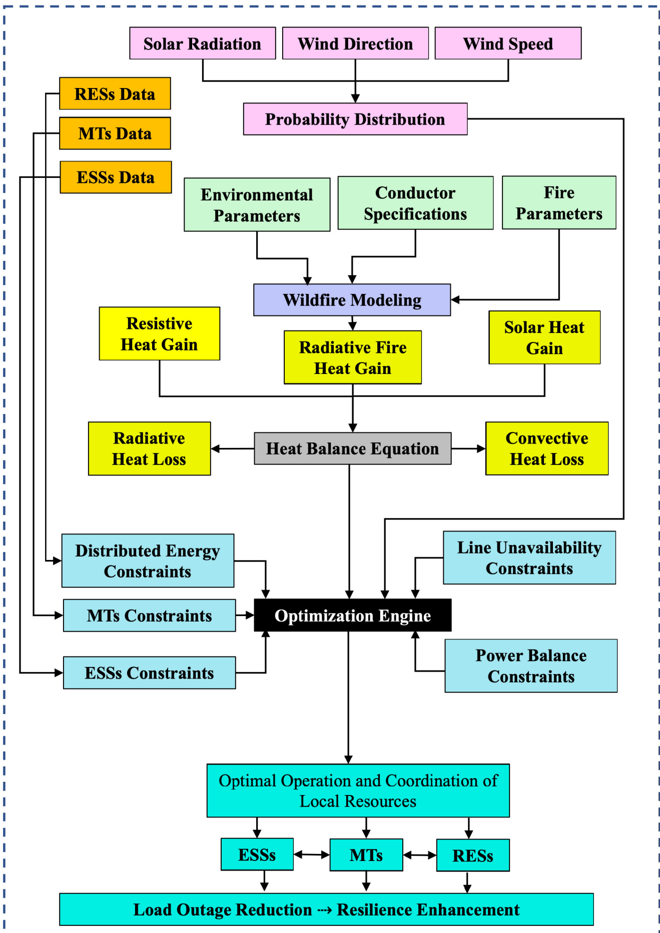

Fig. 1. Big picture of the proposed framework for resilient operation of power distribution networks in the face of wildfire events.

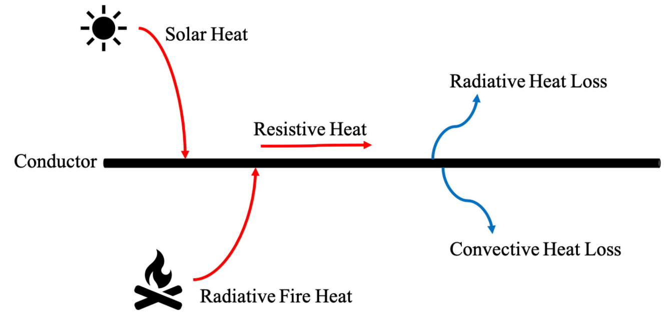

Fig. 2. Illustration of different types of heat gain and heat loss for an overhead line conductor in the event of a wildfire.

Further details on each of the presented steps are provided in the following.

III. Wildfire Modeling Formulation

A. Wildfire Model

The applied wildfire model used in this article is comprehensively introduced for the first time in [8]. Wildfire heat is transferred through radiation and convection. Convective transmission is not of concern in this article, since it influences the temperature of the conductors only when the fire is exactly under the overhead line. It is worth to mention that this article does not consider moderate to extreme wildfires that can burn the conductors and power line towers. Instead, small wildfires with short flame length and small rate of spread are considered to model the effect of heat transferred from wildfire to the conductors when fires are not in a very close distance to the overhead conductors. The radiative heat flux χ^f from the entire flame transmitted to a conductor is then calculated using the geometry of the flame and the fire front properties as follows:

$$\chi^f_{ij,\omega,t} = \frac{\tau \cdot \varepsilon^f \cdot B \cdot {T^f}^4}{2} \cdot \sin(\theta^f_{ij,\omega,t}) \tag{1}$$

where τ, ε^f, and B are all parameters related to the environment. T^f is the temperature of the fire front set as 1200 K [17], and θ^f is the view angle between the threatened line and the fire front expressed in the following.

$$\theta^f_{ij,\omega,t} = \tan^{-1}\left(\frac{\nu^f \cdot \cos(\alpha^f)}{d^f_{ij,\omega,t} - (\nu^f \cdot \sin(\alpha^f))}\right) \tag{2}$$

where ν^f represents the length of the fire and d^f indicates the distance between wildfire and the affected conductor, which is computed in (3)

$$d^f_{ij,\omega,t} = d^f_{ij,\omega,t-1} \cdot V^f_{\omega,t} \cdot \Delta t \cdot \cos(\sigma^{\text{wind}}_{ij,\omega,t}) \tag{3}$$

$$V^f_{\omega,t} = \frac{k \cdot (1 + V^{\text{wind}}_{\omega,t})}{\rho^b}. \tag{4}$$

According to [14], V^f (m/s) is the rate of flame spread in wildland on a flat ground that depends on the wind speed V^{wind}(m/s). ρ^b is the bulk density of the fuel equal to 40 kg/m^3 in the forest. k is equal to 0.07 for wildland fire [7].

B. On the Concept of DHB

According to [8], the power line conductor's total heat is the multiplication of coefficients and heat loss rates—i.e., the convective heat loss rate q^{con}, the radiative heat loss rate q^{rad}—, as well as heat gain rates—i.e., ohmic losses resistance of the power line q^{line}, radiative heat flux from fire q^{fire}, and solar heat gain rate q^{sun}. Fig. 2 illustrates different types of heat gains and losses for a power line conductor. Therefore, any changes in the temperature at any time interval is calculated using the following nonsteady-state heat equation:

$$\begin{aligned}(T_{ij,\omega,t+1} - T_{ij,\omega,t}) = \frac{\Delta t}{mC_p} \cdot (&q^{\text{line}}_{ij,\omega,t} + q^{\text{sun}}_{ij,\omega,t} + q^{\text{fire}}_{ij,\omega,t} \\ &- q^{\text{con}}_{ij,\omega,t} - q^{\text{rad}}_{ij,\omega,t}).\end{aligned} \tag{5}$$

Each of the above terms are explained as follows.

1) Heat Gain: In the given equation, the heating terms are the solar heat energy that the conductor can absorb, the resistive thermal energy produced by currents flowing through the power line conductor, and the fire radiation heat measured as follows:

$$q^{\text{sun}}_{ij,\omega,t} = D_{ij} \cdot \partial_{ij} \cdot \phi^{\text{sun}}_{ij,\omega,t} \tag{6}$$

Authorized licensed use limited to: The George Washington University. Downloaded on August 05,2022 at 03:56:01 UTC from IEEE Xplore. Restrictions apply.

$$q^{\text{line}}_{ij,\omega,t} = R^{\text{line}}(T_{ij,\omega,t}) \cdot (I_{ij,\omega,t})^2 \tag{7}$$

$$q^{\text{fire}}_{ij,\omega,t} = D_{ij} \cdot \chi^{f}_{ij,\omega,t}. \tag{8}$$

In (6), D_{ij} is the diameter of the conductors and $\phi^{\text{sun}}_{ij,\omega,t}$ is the sun radiation rate. ∂_{ij} is the solar absorptivity that varies between 0.27 for the bright stranded aluminum conductor and 0.95 for the weathered conductor in an industrial environment. A value of 0.5 is often used if nothing is known about the conductor absorptivity [18]. In (7), $R^{\text{line}}(T_{ij,\omega,t})$ reflects a function that describes the relationship between the resistance of the power line conductor and its temperature which can be defined as (9), where $R_{ij,a}$ is the resistance of the line at ambient temperature T^a ($298K$). d_{ij} is the conductor thermal resistant coefficient

$$R^{\text{line}}(T_{ij,\omega,t}) = R_{ij,a} \cdot (1 + d_{ij} \cdot (T_{ij,\omega,t} - T^a)). \tag{9}$$

2) Heat Loss: The last two terms in (5) account for the cooling down of the power line conductor. The convection loss in this article is considered as the conductor is cooled down via a cylinder of moving air around the conductor. The convection heat loss is the largest value between high-speed wind $q^{\text{con}}_{ij,\omega,t,(1)}$ and low-speed wind $q^{\text{con}}_{ij,\omega,t,(2)}$ according to the IEEE standard [19]. Equations (10) and (11) represent the calculation of the convection loss

$$q^{\text{con}}_{ij,\omega,t,(1)} = K_{\text{angle}} \cdot 0.754 \cdot N^{0.6}_{Re} \cdot k^a \cdot (T_{ij,\omega,t} - T^a) \tag{10}$$

$$q^{\text{con}}_{ij,\omega,t,(2)} = K_{\text{angle}} \cdot [1.01 + 1.35 \cdot N^{0.52}_{Re}] \cdot k^a \cdot (T_{ij,\omega,t} - T^a). \tag{11}$$

The magnitude of the equation depends on N_{Re}, the Reynolds number and wind direction factor K_{angle} given by

$$N_{\text{Re}} = \frac{D_{ij} \cdot \rho^{\alpha} \cdot V^{\text{wind}}_{\omega,t}}{\mu^{\alpha}} \tag{12}$$

$$\begin{aligned} K_{\text{angle}} &= 1.194 - \cos(\sigma^{\text{wind}}_{ij,\omega,t}) + 0.194\cos(2\sigma^{\text{wind}}_{ij,\omega,t}) \\ &\quad + 0.368\sin(2\sigma^{\text{wind}}_{ij,\omega,t}). \end{aligned} \tag{13}$$

Next, the cable radiated heat rate can be described by the following equation:

$$q^{\text{rad}}_{ij,\omega,t} = 17.8D^{ij} \cdot \epsilon \cdot \left[\left(\frac{T_{ij,\omega,t}}{100} \right)^4 - \left(\frac{T^a}{100} \right)^4 \right]. \tag{14}$$

More detailed information is available in [8] and [20].

IV. Problem Formulation

A. Optimization Model for Wildfire Mitigation

Based on [8] and [20], an optimization model is provided to boost the power distribution system resilience in the face of progressive wildfires. Although resilience is directly linked to load outages [21], operating costs should also be considered to ensure the most cost-effective solution during the emergency operating conditions when facing a progressive wildfire. Therefore, the objective function introduced in this article is to minimize the expected cost as expressed follows:

$$\begin{aligned} \min \Bigg(&\sum_{t=1}^{T}\sum_{\omega=1}^{\Omega} \pi_\omega \cdot \sum_{i=1}^{B} (\text{VoLL}_i \cdot p^{\text{O}}_{i,\omega,t} - c^D \cdot p^D_{i,\omega,t}) \\ &+ \sum_{t=1}^{T}\sum_{\omega=1}^{\Omega} \pi_\omega \cdot \sum_{i=1}^{B} (c^{\text{MT}} \cdot p^{\text{MT}}_{i,\omega,t}) + \sum_{t=1}^{T}\sum_{i=1}^{B} (su^{\text{MT}}_{i,t} + sd^{\text{MT}}_{i,t}) \\ &+ \sum_{t=1}^{T}\sum_{\omega=1}^{\Omega} \pi_\omega \cdot c^{\text{UP}}_t \cdot (p^{\text{UP}_B}_{\omega,t} - p^{\text{UP}_S}_{\omega,t}) \Bigg). \end{aligned} \tag{15}$$

In the first line, π_ω is the probability of each scenario, $\text{VoLL}_i \cdot p^{\text{O}}_{i,\omega,t}$ represents the load outage cost and $c^D \cdot p^D_{i,\omega,t}$ indicates the revenue from providing energy to the end customers. The second and third terms represent the generation, start-up, and shut down costs of MTs. The last term represents the power exchange cost with the upstream network. For simplicity, all costs associated to ESSs, e.g., degradation costs, as well as RESs operation costs are not considered in this article as such costs are far smaller values compared to other cost terms in the objective function [22]. To optimally operate the power distribution network during a progressive wildfire event, multiple constraints should be considered as described in the following.

1) Distributed Energy Resource Constraints: RESs, i.e., wind and solar energy, can be employed in the distribution network to supply some portions of the load demands across the network. According to [8], Weibull distribution is considered for both wind speed and wind direction while normal distribution is considered for solar radiation. Suppose that the wind speed V^{wind} is a stochastic quantity with the following probability density function:

$$f(V^{\text{wind}}) = \frac{K^0}{C^k} \cdot V^{K^0-1} \cdot e^{(-V/C)^{K^0}} \tag{16}$$

where K^0 and C are the shape index and the scale index of the Weibull distribution. In this article, a k-factor of 2 and standard deviation equal to 15% of the mean value are considered for wind speed and direction as well as solar illumination, which can be used as inputs to the optimization engine. The relationship between the output power of a wind generating unit and the wind speed can be formulated as follows:

$$p^{\text{WT}}_{i,t} = 0, \quad 0 \le V \le V_{ci} \;\; \text{or} \;\; V_{co} \le V \qquad \forall i \in \mathbf{B}, t \in \mathbf{T} \tag{17}$$

$$p^{\text{WT}}_{i,t} = P^w_{\text{r}} \cdot \left(\frac{V - V_{ci}}{V_r - V_{ci}} \right), V_{ci} \le V \le V_r \quad \forall i \in \mathbf{B}, t \in \mathbf{T} \tag{18}$$

$$p^{\text{WT}}_{i,t} = P^w_{\text{r}}, \quad V_r \le V \le V_{co} \qquad \forall i \in \mathbf{B}, t \in \mathbf{T} \tag{19}$$

where V is the wind speed at the hub height of the wind unit; V_{ci}, V_{co}, and V_r are, respectively, the cut-in wind speed, the cut-out wind speed, and the rated wind speed; and P^w_{r} is the rated output power of the wind unit [23]. It is worth mentioning that this article does not consider the temporal and spatial correlation of

Authorized licensed use limited to: The George Washington University. Downloaded on August 05,2022 at 03:56:01 UTC from IEEE Xplore. Restrictions apply.

wind farms and, accordingly, the same wind predication data is considered for all wind farms since the distribution system covers a small geographic region.

Regarding the solar power, the illumination intensity is usually considered the dominant factor affecting the output power of the solar panel. The relationship between the illumination intensity and the output power of a solar generating unit can be described as follows:

$$p_{i,t}^{S} = P_{\mathrm{r}}^{S} \cdot \left(\frac{S}{S_r}\right), \quad 0 \leq S \leq S_r, \forall i \in \mathbf{B}, t \in \mathbf{T} \tag{20}$$

$$p_{i,t}^{S} = P_{\mathrm{r}}^{S}, \quad S_r \leq S, \forall i \in \mathbf{B}, t \in \mathbf{T} \tag{21}$$

where S is the illumination intensity, S_r is the rated value, and P_{r}^{S} indicates the rated output power of the solar cells.

2) MTs Constraints: The active and reactive output power of MTs and their start-up and shut-down costs have to be considered as follows to guarantee the power balance in the system at the minimum cost.

$$p_{i(\min)}^{\mathrm{MT}} \cdot \kappa_{i,t} \leq p_{i,\omega,t}^{\mathrm{MT}} \leq p_{i(\max)}^{\mathrm{MT}} \cdot \kappa_{i,t} \forall i \in \mathbf{B}, \omega \in \mathbf{\Omega}, t \in \mathbf{T} \tag{22}$$

$$q_{i(\min)}^{\mathrm{MT}} \cdot \kappa_{i,t} \leq q_{i,\omega,t}^{\mathrm{MT}} \leq q_{i(\max)}^{\mathrm{MT}} \cdot \kappa_{i,t} \forall i \in \mathbf{B}, \omega \in \mathbf{\Omega}, t \in \mathbf{T} \tag{23}$$

$$sd_{i,t}^{\mathrm{MT}} \geq 0, sd_{i,t}^{\mathrm{MT}} \geq c_i^{sd} \cdot (\kappa_{i,t-1} - \kappa_{i,t}) \forall i \in \mathbf{B}, t \in \mathbf{T} \tag{24}$$

$$su_{i,t}^{\mathrm{MT}} \geq 0, \ su_{i,t}^{\mathrm{MT}} \geq c_i^{su} \cdot (\kappa_{i,t} - \kappa_{i,t-1}) \forall i \in \mathbf{B}, t \in \mathbf{T} \tag{25}$$

where (22) and (23) determine the maximum and minimum limits for active and reactive power of MTs, respectively; equations (24) and (25) reflect the start up and shut down costs of the MTs, respectively. The binary variable $\kappa_{i,t}$ is used to determine the status of MTs, e.g., 1 for start up and 0 for shut down, which ensures that if there is a change of status at any time interval, only either start-up or shut-down cost is accounted for in the total cost in the objective function. According to [24], it is considered that the start-up cost parameter, i.e., c^{su}, is 10 times greater than the shut-down cost parameter, i.e., c^{sd}. Besides, the startup/shutdown time of MTs is highly dependent on the size, type, manufacturer, environmental conditions, etc. For the sake of simplicity, this article does not consider the start-up/shut-down time of MTs as the test case is a distribution system and the focus is to temporarily supply the customers as quickest as possible in the face of a wildfire incident.

3) ESSs Constraints: The operation constraints of ESSs can be expressed as follows:

$$\mathrm{SoC}_{i,\omega,t}^{ST} = \mathrm{SoC}_{i,\omega,t-1}^{ST} + \left(\frac{\eta_i^{ST} \cdot p_{i,\omega,t}^{\mathrm{Ch}} \cdot (\frac{\Delta t}{3600})}{E_i^{ST}}\right) - \left(\frac{p_{i,\omega,t}^{\mathrm{dCh}} \cdot (\frac{\Delta t}{3600})}{\eta_i^{ST} \cdot E_i^{ST}}\right) \quad \forall i \in \mathbf{B}, \omega \in \mathbf{\Omega}, t \in \mathbf{T} \tag{26}$$

$$\mathrm{SoC}_{i,(\min)}^{ST} \leq \mathrm{SoC}_{i,\omega,t} \leq \mathrm{SoC}_{i,(\max)}^{ST} \quad \forall i \in \mathbf{B}, \omega \in \mathbf{\Omega}, t \in \mathbf{T} \tag{27}$$

$$0 \leq p_{i,\omega,t}^{\mathrm{Ch}} \leq p_{i,\omega,t,(\max)}^{\mathrm{Ch}} \cdot u_{i,\omega,t} \quad \forall i \in \mathbf{B}, \omega \in \mathbf{\Omega}, t \in \mathbf{T}$$

$$0 \leq p_{i,\omega,t}^{\mathrm{dCh}} \leq \eta_i^{ST} \cdot p_{i,\omega,t,(\max)}^{\mathrm{dCh}} \cdot (1 - u_{i,\omega,t}) \tag{28}$$

$$\forall i \in \mathbf{B}, \omega \in \mathbf{\Omega}, t \in \mathbf{T} \tag{29}$$

$$q_{i(\min)}^{\mathrm{ESS}} \leq q_{i,\omega,t}^{\mathrm{ESS}} \leq q_{i(\max)}^{\mathrm{ESS}} \forall i \in \mathbf{B}, \omega \in \mathbf{\Omega}, t \in \mathbf{T} \tag{30}$$

$$\mathrm{SoC}_{i,\omega,t_{\mathrm{end}}}^{ST} \geq \mathrm{SoC}_{\mathrm{thre}} \forall i \in \mathbf{B}, \omega \in \mathbf{\Omega}. \tag{31}$$

In the equations above, (26) calculates the SoC of ESSs. The limitation on the SoC of ESSs is set by (27). Constraints (28) and (29) guarantee that the active charged or discharged power by ESSs is within the limits considering their operation mode. Note that the binary variable $u_{i,\omega,t}$ is inherently correlated to SoC of ESSs as shown in constraints (26)–(29). Constraint (30) represents the reactive power limits of ESSs. Constraint (31) is to ensure that the SoC of ESSs is above a certain threshold, i.e., $\mathrm{SoC}_{\mathrm{thre}}$, at the end of the simulation. η_i^{ST} is the conversion efficiency of the ESSs, E_i^{ST} represents the energy capacity, $p_{i,\omega,t}^{\mathrm{Ch}}$ and $p_{i,\omega,t}^{\mathrm{dCh}}$ are, respectively, the charging and discharging active power of the ESS, and Δt is the duration of time intervals.

4) Power Balance Constraints: Each node should maintain a real and reactive power balance between the generated power and the demanded electricity.

$$\sum_{j=1}^{B_i} P_{ij,\omega,t}^{\mathrm{fl}} = p_{i,\omega,t}^{\mathrm{MT}} + p_{i,\omega,t}^{\mathrm{WT}} + p_{i,\omega,t}^{S} + p_{\omega,t}^{\mathrm{UP}} + p_{i,\omega,t}^{\mathrm{Ch}} - p_{i,\omega,t}^{\mathrm{dCh}} - p_{i,\omega,t}^{D} \quad \forall i \in \mathbf{B}, \omega \in \mathbf{\Omega}, t \in \mathbf{T} \tag{32}$$

$$\sum_{j=1}^{B_i} Q_{ij,\omega,t}^{\mathrm{fl}} = q_{i,\omega,t}^{\mathrm{MT}} + q_{i,\omega,t}^{\mathrm{ESS}} - q_{i,\omega,t}^{D} \quad \forall i \in \mathbf{B}, \omega \in \mathbf{\Omega}, t \in \mathbf{T}$$

$$-\bar{P}_{ij,t}^{\mathrm{fl}} * \alpha_{ij,\omega,t} \leq P_{ij,\omega,t}^{\mathrm{fl}} \leq \bar{P}_{ij,t}^{\mathrm{fl}} * \alpha_{ij,\omega,t} \tag{33}$$

$$\forall ij \in \mathbf{L}, \omega \in \mathbf{\Omega}, t \in \mathbf{T}$$

$$-\bar{Q}_{ij,t}^{\mathrm{fl}} * \alpha_{ij,\omega,t} \leq Q_{ij,\omega,t}^{\mathrm{fl}} \leq \bar{Q}_{ij,t}^{\mathrm{fl}} * \alpha_{ij,\omega,t} \tag{34}$$

$$\forall ij \in \mathbf{L}, \omega \in \mathbf{\Omega}, t \in \mathbf{T}. \tag{35}$$

Constraints (34) and (35) allow the power flow through each line only when $\alpha_{ij,\omega,t}$ is equal to 1 meaning the line is online. It should be noted that this article considers that the capacity limit of the lines does not change with the temperature in real time. The thermal capacity limits are predefined parameters in advance to running the optimization problem.

The variables $p_{i,\omega,t}^{D}$ and $q_{i,\omega,t}^{D}$ are the supplied active and reactive power to the customers, which are calculated by the load outage $p_{i,\omega,t}^{\mathrm{O}}$ subtracted from the original demand at each node $P_{i,\omega,t}^{\mathrm{demand}}$ in (36) and (37)

$$p_{i,\omega,t}^{D} = P_{i,\omega,t}^{\mathrm{demand}} - p_{i,\omega,t}^{\mathrm{O}} \quad \forall i \in \mathbf{B}, \omega \in \mathbf{\Omega}, t \in \mathbf{T} \tag{36}$$

$$q_{\omega,t}^{D} = Q_{i,\omega,t}^{\mathrm{demand}} - q_{i,\omega,t}^{\mathrm{O}} \quad \forall i \in \mathbf{B}, \omega \in \mathbf{\Omega}, t \in \mathbf{T} \tag{37}$$

$$0 \leq p_{i,\omega,t}^{\mathrm{O}} \leq P_{i,\omega,t}^{\mathrm{demand}} \quad \forall i \in \mathbf{B}, \omega \in \mathbf{\Omega}, t \in \mathbf{T} \tag{38}$$

Authorized licensed use limited to: The George Washington University. Downloaded on August 05,2022 at 03:56:01 UTC from IEEE Xplore. Restrictions apply.

$$q^{\mathrm{O}}_{i,\omega,t} = p^{\mathrm{O}}_{i,\omega,t} \cdot \frac{Q^{\mathrm{demand}}_{i,\omega,t}}{P^{\mathrm{demand}}_{i,\omega,t}} \qquad \forall i \in \mathbf{B}, \omega \in \mathbf{\Omega}, t \in \mathbf{T}. \tag{39}$$

In (32), the active power $p^{\mathrm{UP}}_{\omega,t}$ represents the power exchange with the upstream network during the optimization horizon. It depends on the energy purchases from or sold to the main grid and needs to be limited as shown in (40)–(42). The binary variable $\varphi^{\mathrm{UP}}_{\omega,t}$ is used to determine buying (1) or selling (0) energy during the considered time horizon

$$p^{\mathrm{UP}}_{\omega,t} = p^{\mathrm{UP_{buy}}}_{\omega,t} - p^{\mathrm{UP_{sell}}}_{\omega,t} \qquad \forall \omega \in \mathbf{\Omega}, t \in \mathbf{T} \tag{40}$$

$$0 \leq p^{\mathrm{UP_{buy}}}_{\omega,t} \leq p^{\mathrm{UP_{buy}}}_{\max} \cdot \varphi^{\mathrm{UP}}_{\omega,t} \qquad \forall \omega \in \mathbf{\Omega}, t \in \mathbf{T} \tag{41}$$

$$0 \leq p^{\mathrm{UP_{sell}}}_{\omega,t} \leq p^{\mathrm{UP_{sell}}}_{\max} \cdot (1 - \varphi^{\mathrm{UP}}_{\omega,t}) \qquad \forall \omega \in \mathbf{\Omega}, t \in \mathbf{T}. \tag{42}$$

5) DHB Constraints: The following constraints determine the temperature rise of overhead power line conductors impacted by the radiated heat flux of a progressive wildfire.

$$(T_{ij,\omega,t+1} - T_{ij,\omega,t}) = \frac{\Delta t}{mC_p} \cdot [(q^{\mathrm{line}}_{ij,\omega,t} + q^{\mathrm{sun}}_{ij,\omega,t} + q^{\mathrm{fire}}_{ij,\omega,t} - q^{\mathrm{con}}_{ij,\omega,t} - q^{\mathrm{rad}}_{ij,\omega,t})] \qquad \forall ij \in \ell, \omega \in \mathbf{\Omega}, t \in \mathbf{T} \tag{43}$$

$$q^{\mathrm{sun}}_{ij,\omega,t} = D_{ij} \cdot \partial_{ij} \cdot \phi^{\mathrm{sun}}_{ij,,\omega,t} \qquad \forall ij \in \ell, \omega \in \mathbf{\Omega}, t \in \mathbf{T} \tag{44}$$

$$q^{\mathrm{line}}_{ij,\omega,t} = R^{\mathrm{line}}(T_{ij,\omega,t}) \cdot (I_{ij,\omega,t})^2 \qquad \forall ij \in \ell, \omega \in \mathbf{\Omega}, t \in \mathbf{T} \tag{45}$$

$$q^{\mathrm{fire}}_{ij,\omega,t} = D_{ij} \cdot \chi^{f}_{ij,\omega,t} \qquad \forall ij \in \ell, \omega \in \mathbf{\Omega}, t \in \mathbf{T} \tag{46}$$

$$q^{\mathrm{con}}_{ij,\omega,t} = \max \begin{pmatrix} K_{\mathrm{angle}} \cdot [1.01 + 1.35 \cdot N^{0.52}_{Re}] \cdot k^a \cdot (T_{ij,\omega,t} - T^a) \\ K_{\mathrm{angle}} \cdot 0.754 \cdot N^{0.6}_{Re} \cdot k^a \cdot (T_{ij,\omega,t} - T^a) \end{pmatrix}$$

$$q^{\mathrm{rad}}_{ij,\omega,t} = 17.8 D_{ij} \cdot \epsilon \cdot \left[\left(\frac{T_{ij,\omega,t}}{100} \right)^4 - \left(\frac{T^a}{100} \right)^4 \right] \tag{47}$$

$$\forall ij \in \ell, \omega \in \mathbf{\Omega}, t \in \mathbf{T} \tag{48}$$

$$T_{ij,\omega,t} \leq T^{\max} + (1 - \alpha_{ij,\omega,t}) * M \quad \forall ij \in \ell, \omega \in \mathbf{\Omega}, t \in \mathbf{T} \tag{49}$$

$$\alpha_{ij,\omega,t} \leq \alpha_{ij,\omega,t-1} \qquad \forall ij \in \ell, \omega \in \mathbf{\Omega}, t \in \mathbf{T}. \tag{50}$$

Constraint (43) indicates the nonsteady-state heat balance equation. Constraints (44)–(46) show the heat gain by the conductor, whereas constraints (47) and (48) demonstrate the heat loss by the conductor. Constraint (49) reflects that when the conductor temperature surpasses the maximum permitted temperature, the associated overhead line will become out of service. Once the overhead line gets unavailable, it will remain out of service then after as indicated in constraint (50).

B. Convexification and Linearization

The heat gain due to the ohmic losses presented in (45), is the multiplication of current flow square and conductor resistance. For an ohmic conductor, as shown in (9), the resistance can be calculated by a function of conductor temperature. In order to convexify the heat caused by the current, we consider that the resistance of the conductor is a constant value equal to its maximum at the highest temperature $T^{\max}$. Also, the voltage is considered close to 1 p.u.. Applying this method, the current flow is equal to the apparent power flow and constraint (45) is relaxed to the following inequality [25]:

$$q^{\mathrm{line}}_{ij,\omega,t} \geq R^{\mathrm{line}}(T^{\max}) \cdot (|P^{\mathrm{fl}}_{ij,\omega,t}|^2 + |Q^{\mathrm{fl}}_{ij,\omega,t}|^2). \tag{51}$$

The radiation heat loss depends on the fourth power of the conductor temperature as shown in (48). According to [25], the radiative heat loss rate can be linearly approximated as

$$q^{\mathrm{rad}}_{ij,\omega,t} = a \cdot T_{ij,\omega,t} + b \tag{52}$$

where $a = 0.9517$ and $b = -269.98$ are the coefficients used in the radiated heat loss rate.

Based on the DistFlow branch equations in [26], constraint (53) and (54) represent the power flow equation. The large-enough positive number M is a relaxation parameter to relax these two constraints for open (offline) branches. Constraint (55) states the boundary for the nodal voltage magnitudes across the power distribution network

$$V_{\mathrm{sqr}\,i,\omega,t} - V_{\mathrm{sqr}\,j,\omega,t} \leq (1 - \alpha_{ij,\omega,t}) \cdot M + 2 \cdot (r_{ij} \cdot P^{\mathrm{fl}}_{ij,\omega,t} + x_{ij} \cdot Q^{\mathrm{fl}}_{ij,\omega,t}), \quad \forall ij \in \mathbf{L}, \omega \in \mathbf{\Omega}, t \in \mathbf{T} \tag{53}$$

$$V_{\mathrm{sqr}\,i,\omega,t} - V_{\mathrm{sqr}\,j,\omega,t} \geq (\alpha_{ij,\omega,t} - 1) \cdot M + 2 \cdot (r_{ij} \cdot P^{\mathrm{fl}}_{ij,\omega,t} + x_{ij} \cdot Q^{\mathrm{fl}}_{ij,\omega,t}), \quad \forall ij \in \mathbf{L}, \omega \in \mathbf{\Omega}, t \in \mathbf{T} \tag{54}$$

$$\underline{V_{\mathrm{sqr}}}_i \leq V_{\mathrm{sqr}\,i,\omega,t} \leq \overline{V_{\mathrm{sqr}}}_i, \qquad \forall i \in \mathbf{B}, \omega \in \mathbf{\Omega}, t \in \mathbf{T}. \tag{55}$$

V. Case Study and Numerical Results

A. Test System Characteristics and Simulation Data

A modified IEEE 33-node test system [27] is considered to illustrate the effectiveness of the mitigation framework for resilient operation of power distribution grids when facing wildfires. The single-line diagram of the considered test system is illustrated in Fig. 3. The test system is assumed to be a balanced distribution grid with active peak demand equal to 13.35 MW. Since the distribution grid covers a small geographical area, its components are all subjected to similar environmental conditions. The location of ESSs, MTs, and RESs are depicted in Fig. 3. According to [8], the capacity of WTs, PVs, MTs, and the ESSs are tabulated in Table I. The electricity price and the power demand are depicted in Fig. 4. It is assumed that buying and selling energy from/to the upstream network has the same price. The value of lost load (VoLL) is randomly generated between 1000 to 5000 MWh to prioritize the critical loads [28]. It is considered that the price of selling energy to end customers is 270 \$/MWh, the operation cost of MTs is 80 \$/MWh, and the start-up and

Authorized licensed use limited to: The George Washington University. Downloaded on August 05,2022 at 03:56:01 UTC from IEEE Xplore. Restrictions apply.

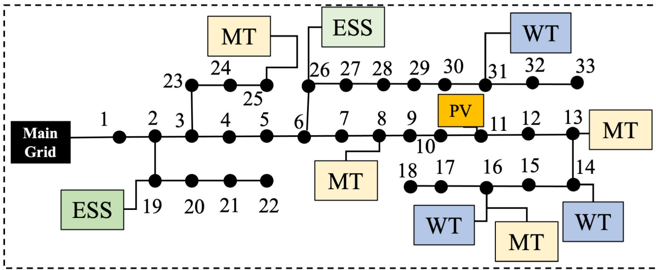

Fig. 3. Modified IEEE 33-node test system: The studied test system extracted from [8].

TABLE I
CAPACITY OF ESSS, RESSS, AND MTS

Element	Node	Capacity (MW)
ESS	19/26	0.5/0.5
PV	11	0.55
WT	14/16/31	0.85
MT	8/13/16/25	3/2/2/3

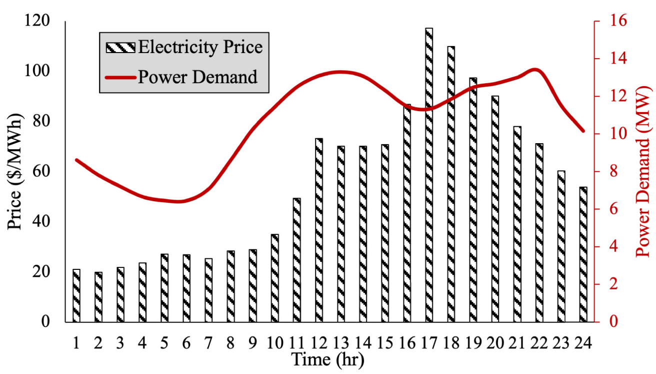

Fig. 4. Power demand and the electricity exchange price.

shut-down costs of MTs are, respectively, 300 $/MWh and 30 $/MWh. The cut-in, cut-out, and rated wind speeds for WTs are 4, 20, and 12 m/s, respectively. The PVs have a rated illumination intensity of 1000 $\mathrm{W/m^2}$ and the solar radiation has the mean value of 316 $\mathrm{W/m^2}$. The weather parameters and wildfire information are derived from [7] and the wind and solar data are taken from [29], [30]. The standard deviation is calculated to be 15% of the mean value for wind speed and solar radiation. The time step is considered 1 h and the studied emergency horizon is 24 h. The initial distance of the fire from the affected power lines are assumed as 1000 m and it is also assumed that the affected lines will be out of service until the end of the time horizon (i.e., until which the fire will be suppressed). The SoC of the ESSs is expected to remain greater than 30% of the full potential at the end of the simulation time, in order to further contribute to demand fulfillment for the next hours beyond the analysis time horizon. An ACSR type of power line conductor is considered. The diameter and the emissivity of conductors are considered as 28 mm and 0.5, respectively. The maximum acceptable temperature of the power line is considered 353 K. All other data can be found in [8] and [20]. The optimization

TABLE II
SIMULATION RESULTS: BENCHMARK CASE

# of Scenarios	Objective Function ($\$\times10^3$)	Load outage Cost ($\$\times10^3$)	Computation Time (s)
10	-30.25	25.00	75
100	-33.14	22.23	1080
500	-31.57	22.57	3750

problem runs on a programming platform using CPLEX solver to handle the mixed integer quadratic programming formulation. A General Algebraic Modeling System (GAMS) environment, using a PC with an Intel Xeon E5-2620 v2 processor, 16 GB of memory, and 64-b operating system is used to solve and numerically analyze the results.

B. Resilient Operation of the Test System

Different number of scenarios have to be considered to account for the inherent variability of the stochastic parameters, i.e., *wind speed*, *wind direction*, and *solar radiation*. All stochastic parameters are here considered uncorrelated. The same uniform environmental conditions are applied to the test system as power distribution test systems usually cover a small geographical region. For the *Benchmark Case*, it is assumed that the wildfire approaches overhead lines 1–2 and 2–3. The radiative heat flux emitted from the wildfire can change with the wind speed and direction as explained in equations (1)–(4). Wildfire spread rate is also highly dependent on wind speed according to (4). Solar radiation as a source of heat gain can also change the temperature of the conductors. Therefore, different number of scenarios representing stochastic parameters will result in different temperature rise of conductors and change the optimal solution. Different simulation results are tabulated in Table II. One can observe that increasing the number of scenarios changes the computation time significantly, while there is no much difference neither in the the objective function nor in the expected value of the load shedding outcome. Considering the fact that the applied approach is used when a wildfire impacts the power distribution system and prompt judgments and swift decisions are required, 10 number of scenarios appear to be the best option to represent the variation in the stochastic parameters. For 10 number of scenarios, the optimization is solved in 75 s, quick enough to satisfy the requirement of a rapid response, while the objective function and the load outage remain almost the same as that in the other cases when more number of scenarios are considered. Therefore, for the following analyses in this article, only 10 number of uncertainty scenarios are considered. Fig. 5 shows the box-plot of the wind speed with Weibull distribution for 10 number of scenarios. It can be observed that for instance, at time 21:00, the minimum, median, and maximum value of the wind speed are, respectively: 7.5, 11.80, and 16.07 m/s.

For the *Benchmark Case,* where the fire hits overhead lines 1–2 and 2–3 for example, the wildfire is assumed to be ignited at time 18:00 with the initial distance of 1000 m with overhead lines 1–2 and 2–3. The conductor temperature of the lines 1–2 and 2–3 is obviously higher than other conductors since the flow

Authorized licensed use limited to: The George Washington University. Downloaded on August 05,2022 at 03:56:01 UTC from IEEE Xplore. Restrictions apply.

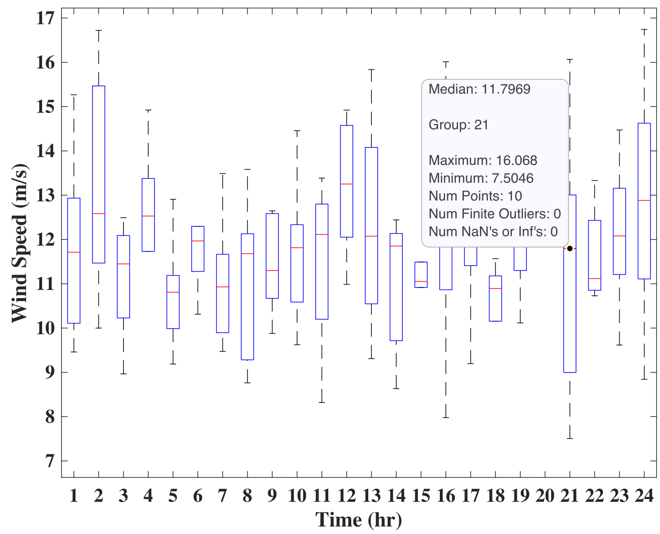

Fig. 5. Box-plot of wind speed for different time periods and for 10 number of scenarios: Benchmark Case.

TABLE III
EXPECTED CONDUCTOR TEMPERATURE OF IMPACTED LINES FOR AN APPROACHING WILDFIRE: BENCHMARK CASE

	Conductor Temperature (K)								
Line	t_{13}	t_{14}	t_{15}	t_{16}	t_{17}	t_{18}	t_{19}	t_{20}	$t \geq 21$
1-2	315	316	317	320	323	327	331	348	Out
2-3	314	316	317	319	321	324	329	349	Out

of electricity in these lines is higher. The temperature profiles of overhead lines 1–2 and 2–3 are obtained in Table III. One can observe that the conductor temperature of lines 1–2 and 2–3 increases slightly after 13:00 since the ambient temperature starts increasing; however, there is a jump in the conductor temperature at 19:00 when the fire reaches to a closer distance, e.g., 500 m. Eventually at 21:00, the conductor temperature exceeds its acceptable safety threshold of 353 K, resulting in the lines becoming out of service then after. Once the overhead line becomes out of service, the conductor temperature can be cooled down as the resistive heat is taken out from the sources of heat for the conductors.

Once overhead power lines 1–2 and 2–3 get unavailable and the power distribution grid becomes isolated from the upstream network, the role of local energy resources, e.g., MTs, RESs, and ESSs, becomes imperative. Portions of demanded loads could be partially or fully supplied by the available local energy resources if their operation decisions are optimally coordinated. The demanded loads, expected generated power by all local energy resources, and the expected load shedding are tabulated in Table IV for $t_{21} - t_{24}$ when overhead lines 1–2 and 2–3 are out of service. During the period of 21:00–24:00, the demanded energy is 48 MWh with the peak of 13.35 MW at 22:00 and the average of 12 MW. It is realized that approximately 83% of all the demanded loads could be supplied by all local energy resources when the grid is isolated from the upstream network *if and only if* each available resource is resiliently operated and optimally coordinated with other resources. In other words, only

TABLE IV
DEMANDED LOAD, GENERATED POWER, AND LOAD OUTAGE: BENCHMARK CASE

	t_{21}	t_{22}	t_{23}	t_{24}
Load Demand (MW)	13	13.35	11.5	10.15
MTs (MW)	6.85	9.05	7.50	6.34
PVs (MW)	0	0	0	0
WTs (MW)	2.02	2.13	2.20	2.21
ESSs (MW)	0.31	0.43	0.40	0.38
Upstream Network (MW)	0	0	0	0
Load Outage (MW)	3.82	1.73	1.40	1.21

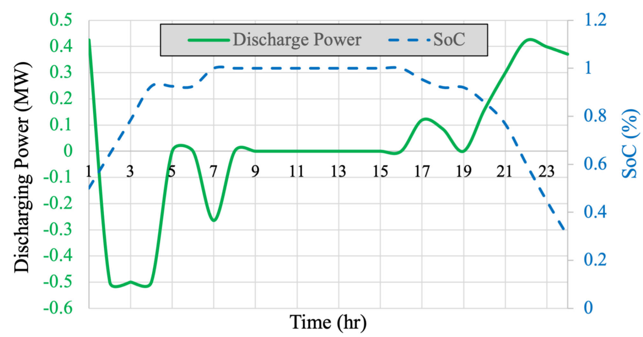

Fig. 6. Expected discharging power and SoC of ESS located at node 19: Benchmark Case.

TABLE V
EXPECTED COSTS AND EXPECTED REVENUE: BENCHMARK CASE

Load Outage Cost ($\$ \times 10^3$)	MTs Generation Cost ($\$ \times 10^3$)	Exchanged Power Cost ($\$ \times 10^3$)	Revenue ($\$ \times 10^3$)
25.00204	6.31496	4.8153	66.383

8.16 MWh of the total 48 MWh demanded loads are not supplied which can be interpreted as 83% *resilience enhancement* in the system. Particularly, one can see that approximately 62% of the loads are supplied by MTs, 18% are supplied by WTs, and 4% are supplied by ESSs discharging during 21:00–24:00. It is also obvious that after t_{21}, and since there is no sun light, PVs cannot contribute to load recovery. However, PVs along with other sources, charge the ESSs to their full capacity so they can be discharged when the distribution grid is isolated from the upstream network. Fig. 6 shows the expected operation profile of ESS located at node 19. One can see that the ESS gets charged from t_1 until t_9 when it gets to its full SoC capacity. Starting at t_{17}, it gets discharged to help reduce the cost of electricity purchase from the upstream network in time intervals when the electricity price is higher. During t_{21}–t_{24}, the ESS also contributes to reducing the load outage and at t_{24}, it reaches to its predefined threshold SoC set to 30%. Table V summarizes the expected value of the load shedding cost, the MTs generation cost, the exchanged power cost with the upstream network, and the revenue from selling energy to the customers. It is observed that the more the outage time, the less revenue from selling energy to the customers and the higher the load shedding cost. In addition, one can observe that although MTs play a big role in restoring the loads, they are expensive solutions. Therefore, to

Authorized licensed use limited to: The George Washington University. Downloaded on August 05,2022 at 03:56:01 UTC from IEEE Xplore. Restrictions apply.

TABLE VI
SENSITIVITY ANALYSES ON THE NUMBER AND LOCATION OF IMPACTED LINES

		Impacted Lines	Cost Function ($ $\times 10^3$)					Load Outage (MWh)	Supplied Loads (%)		
			Total Cost	Load Outage Cost	MTs Cost	Exchanged Power Cost	Revenue		MTs	RESs	ESS
Case I	Bench	1-2 2-3	-30.25	25.00	6.32	4.82	66.38	8.1591	61.97	17.98	3.16
Case I	Sce 2	3-4 4-5	-47.78	8.38	5.70	5.51	67.34	2.9688	51.55	17.98	1.28
Case I	Sce 3	31-32 32-33	-50.51	5.93	4.00	6.90	67.34	3.1549	16.48	17.98	1.47
Case II	Sce 1	1-2 2-3 3-4	-26.02	28.89	6.16	4.83	65.89	8.5349	61.02	17.98	3.31
Case II	Sce 2	8-9 9-10 10-11	-46.47	9.89	4.39	6.59	67.34	3.1549	24.59	17.98	1.47
Case II	Sce 3	2-19 19-20 20-21	-37.64	18.43	4.00	6.84	66.90	4.7769	16.48	17.98	3.26
Case III	Sce 1	1-2 2-3 3-4 4-5	-22.96	31.81	6.11	4.82	65.71	9.2071	59.97	17.98	3.26
Case III	Sce 2	8-9 9-10 10-11 11-12	-40.45	15.56	4.27	6.59	66.92	4.7324	21.99	17.98	1.47
Case III	Sce 3	2-3 3-4 2-19 3-23	-24.22	30.70	6.04	4.93	65.89	8.5349	58.42	17.98	3.31

have an optimal, resilient, and yet cost-effective solution, MTs should be optimally operated and strategically coordinated with RESs and ESSs units.

C. Sensitivity Analyses

1) Sensitivity Analyses on the Number and Location of Impacted Overhead Lines: In order to evaluate the generality of the applied framework, comprehensive sensitivity analyses on the number and location of impacted lines are conducted in this section. Different cases are introduced where in *Case I*, only 2 overhead power lines are impacted by the wildfire event while in *Case II* and *Case III*, three and four lines are, respectively, impacted by the wildfire. It is assumed that the wildfire characteristics do not change when the fire approaches different lines. For each case, three different Scenarios are defined in which the locations of impacted lines are changed randomly. Table VI illustrates the simulation results for all studied Cases and Scenarios. It should be noted that the percentage of supplied loads by each local energy resource, i.e., RESs, MTs, and ESSs, is computed only for the period of times when the impacted lines are unavailable. For instance, in Case I–Scenario 2, 51.55% of all loads are supplied by MTs for the period of 21:00–24:00 when lines 3–4 and 4–5 are out of service. In addition, the load shedding is computed for the entire period of lines unavailability. For example, in Case III–Scenario 1, lines 1–2, 2–3, 3–4, and 4–5 will be out of service during 20:00–24:00 time intervals, where the total load shedding for this period is 9.2071 MWh. One can observe that RESs, e.g., PVs and WTs, always supply 17.98% of the loads during the period of times when the impacted lines are out of service. That is because in all the studied Cases and Scenarios, WTs and PVs are connected to at least one node and the same nodes are always supported by these resources. In other words, WTs located at node 14, 16, 31, supply 674.9739 kW at 21:00, 711.5615 kW at 22:00, 734.5844 kW at 23:00, and 738.8061 kW at 24:00 while the PVs output located at node 11 is always zero for these periods of time. Therefore, since WTs are always available in the considered Scenarios, their contribution in all Cases and Scenarios is the same. It is also observed that the role of MTs is significant in supplying loads in all Cases. Nonetheless, since the MTs are expensive resources, the optimization framework only picks up MTs for supplying loads either when the electricity price is higher than the operation cost of MTs or when there is a critical load outage with high VoLL that could be supplied by MTs. This can be observed in Case I–Scenario 2, where only 16% of loads are supplied by MTs for the period of 21:00–24:00. That is because a big portion of demand can be supplied by either the upstream network or RESs. Particularly in this case, MTs only supply 10 MWh in total for the period of 16:00–20:00, where the electricity price is much higher than other time intervals—see Fig. 4. From Table VI, it is also realized that the load shedding cost in Case III is much higher than that in other cases primarily due to the unavailability of four lines at the same time. However, the total cost of the system does not change exponentially and that is because the

Authorized licensed use limited to: The George Washington University. Downloaded on August 05,2022 at 03:56:01 UTC from IEEE Xplore. Restrictions apply.

TABLE VII
SENSITIVITY ANALYSES RESULTS ON THE NUMBER OF MTS

Number of MTs	MTs Costs ($)	Exchanged Power Cost ($)	Load Outage (MWh)	Supplied Loads by MTs (%)
1	1796	8072	31	17
2	3251	7144	22	34
3	4698	6240	13	51
4	6320	4820	8	62
5	7086	3890	6	63

load outages are really reduced by local energy resources when they are optimally operated and coordinated. For instance, in Case III–Scenario 1, where the load shedding has the highest value, nearly 81.21% of the load demand are supplied by local energy resources during the outage time periods when fire hits the power network. In summary, one can conclude that the optimal operation and coordination of all local energy resources are needed for effective recovery and to enhance the power distribution system resilience when facing wildfire incidents.

2) Sensitivity Analyses on the Number of MTs: This section conducts sensitivity analyses on the number of MTs in the distribution grid as MTs play a major role in supplying loads. Different number of MTs is considered in the network to analyze the MTs associated costs, the exchanged power cost with the upstream network, the total load shedding, and the percentage of supplied loads by MTs. Table VII tabulates the expected value of the results for Benchmark Case when the approaching fire hits lines 1–2 and 2–3 and make them out of service for the period of 21:00–24:00. One can see that by increasing the number of MTs, the operation costs of MTs will increase as expected, while the exchanged power with the upstream network will decrease. That is because during the normal operating time before the wildfire hits the network, when the purchase cost of electricity from the upstream network is higher than the operation costs of MTs and the load demand is less, MTs can generate power not only to supply some portions of the load, but also to sell energy to the upstream network for revenue. Therefore, the more available MTs in the network, the less exchanged power cost and the less load shedding as a consequence. Comparing the studied cases with four and five number of MTs in the system, it is observed that the percentage of load supplied by MTs during 21:00–24:00 does not change significantly. Therefore, four number of MTs seems to be acceptable and sufficient for the studied test system to achieve a resilient operation during wildfire events.

VI. CONCLUSION

This article presented a general framework to enhance the power distribution system's operational resilience in the face of wildfire hazards. In particular, different aspects of wildfire are characterized first where DHB equations were used to mathematically model the impacts of wildfire on overhead power line conductor's temperature. A mitigation optimization model was then introduced that aimed to minimize the load outages and the corresponding consequences in the grid during wildfires. The numerical results revealed that the load outage could be remarkably reduced if the progressive wildfire is characterized in advance and all local energy resources, i.e., RESs, MTs, and ESSs, are strategically and optimally coordinated.

A promising future research direction could be exploring quantitative models that can capture the thermal capacity of the power lines (both transmission and distribution) changing dynamically based on the conductor temperature in the face of a progressive wildfire incident. Another potential future research direction could be on the tradeoff between investing new distributed energy resources, e.g., RESs, ESSs, MTs, in the distribution network and the load outage reduction for more resilience benefits during wildfire emergencies. Also, investigating the characteristics and dynamic behaviour of different types of MTs and exploring the deployment of fast-response MTs for enhancing the power system resilience to wildfires could be pursued. The last but not least potential future research direction could be targetted on the analysis of the spatial-temporal fire behavior, i.e., the fire intensity, flame length, and rate of spread that are dependent on different uncertain variables including ignition time and location, the fuel type, slope, elevation, canopy cover, moisture, wind speed and wind direction, along with other parameters to tackle the inherent and exogenous uncertainties in wildfires behavior.

REFERENCES

[1] S. E. DeYoung, J. Chase, M. P. Branco, and B. Park, "The effect of mass evacuation on infant feeding: The case of the 2016 fort mcmurray wildfire," *Maternal Child Health J.*, vol. 22, no. 12, pp. 1826–1833, 2018.

[2] D. Jones, "October wildfire claims top 9.4 billion statewide," 2017, [Online] Available: http://www.insurance.ca.gov/0400-news/0100-press-releases/2017/release135-17.cfm.

[3] *Times Editorial Board*, "Wildfires are natural disasters but congress refuses to budget for them," *Los Angeles Times*, Jan. 2018, [Online] Available: https://www.latimes.com/opinion/editorials/la-ed-wildfire-funding-fix-20180102-story.html.

[4] US Forest Service Report, "The rising cost of fire operations: Effects on the forest service's non-fire work," US Department of Agriculture, 2015.

[5] Top 10 costliest wildland fires in the United States, [Online] Available: https://www.iii.org/table-archive/21424.

[6] H. Trabish, "De-energize and DERs: The tough options wildfires pose for California utilities," 2019, [Online] Available: https://www.utilitydive.com/news/the-hard-choice-californias-wildfires-have-forced-on-its-utilities-and-a/548614/.

[7] M. Choobineh, B. Ansari, and S. Mohagheghi, "Vulnerability assessment of the power grid against progressing wildfires," *Fire Saf. J.*, vol. 73, pp. 20–28, 2015.

[8] D. N. Trakas and N. D. Hatziargyriou, "Optimal distribution system operation for enhancing resilience against wildfires," *IEEE Trans. Power Syst.*, vol. 33, no. 2, pp. 2260–2271, Mar. 2017.

[9] A. Bagchi, A. Sprintson, and C. Singh, "Modeling the impact of fire spread on an electrical distribution network," *Electric Power Syst. Res.*, vol. 100, pp. 15–24, 2013.

[10] S. Mohagheghi and S. Rebennack, "Optimal resilient power grid operation during the course of a progressing wildfire," *Int. J. Elect. Power Energy Syst.*, vol. 73, pp. 843–852, 2015.

[11] B. Ansari and S. Mohagheghi, "Optimal energy dispatch of the power distribution network during the course of a progressing wildfire," *Int. Trans. Elect. Energy Syst.*, vol. 25, no. 12, pp. 3422–3438, 2015.

[12] J. W. Mitchell, "Power line failures and catastrophic wildfires under extreme weather conditions," *Eng. Failure Anal.*, vol. 35, pp. 726–735, 2013.

[13] D. Coldham, A. Czerwinski, and T. Marxsen, "Probability of bushfire ignition from electric arc faults," HRL Technology Pty Ltd., Melbourne, VIC., Australia, Tech. Rep. HRL/2010/195, 2011.

[14] E. I. Koufakis, P. T. Tsarabaris, J. S. Katsanis, C. G. Karagiannopoulos, and P. D. Bourkas, "A wildfire model for the estimation of the temperature rise of an overhead line conductor," *IEEE Trans. Power Del.*, vol. 25, no. 2, pp. 1077–1082, Apr. 2010.

Authorized licensed use limited to: The George Washington University. Downloaded on August 05,2022 at 03:56:01 UTC from IEEE Xplore. Restrictions apply.

[15] S. Wang and P. Dehghanian, "On the use of artificial intelligence for high impedance fault detection and electrical safety," *IEEE Trans. Ind. Appl.*, vol. 56, no. 6, pp. 7208–7216, Nov./Dec. 2020.
[16] S. Jazebi, F. De Leon, and A. Nelson, "Review of wildfire management techniques-part I: Causes, prevention, detection, suppression, and data analytics," *IEEE Trans. Power Del.*, vol. 35, no. 1, pp. 430–439, Feb. 2020.
[17] J.-L. Rossi, A. Simeoni, B. Moretti, and V. Leroy-Cancellieri, "An analytical model based on radiative heating for the determination of safety distances for wildland fires," *Fire Saf. J.*, vol. 46, no. 8, pp. 520–527, 2011.
[18] I. Z. F. bin Hussien, A. A. Rahim, and N. Abdullah, "Electric power transmission," in *Proc. Altern. Energy Power Electron.*, Elsevier, 2011, pp. 317–347.
[19] "IEEE standard for calculating the current-temperature relationship of bare overhead conductors," *IEEE Std 738-2012 Revision of IEEE Std 738-2006 - Incorporates IEEE Std 738-2012 Cor 1-2013)*, pp. 1–72, 2013.
[20] F. Teng, "Enhancing power distribution grid resilience against massive wildfires," *Master's Thesis*, The George Washington Univ., 2020.
[21] M. Panteli, D. N. Trakas, P. Mancarella, and N. D. Hatziargyriou, "Boosting the power grid resilience to extreme weather events using defensive islanding," *IEEE Trans. Smart Grid*, vol. 7, no. 6, pp. 2913–2922, Nov. 2016.
[22] K. Zou, A. P. Agalgaonkar, K. M. Muttaqi, and S. Perera, "Multi-objective optimisation for distribution system planning with renewable energy resources," in *Proc. IEEE Int. Energy Conf.*, 2010, pp. 670–675.
[23] Z. Liu, F. Wen, and G. Ledwich, "Optimal siting and sizing of distributed generators in distribution systems considering uncertainties," *IEEE Trans. power Del.*, vol. 26, no. 4, pp. 2541–2551, Oct. 2011.
[24] T. Xu, A. B. Birchfield, K. M. Gegner, K. S. Shetye, and T. J. Overbye, "Application of large-scale synthetic power system models for energy economic studies," in *Proc. 50th Hawaii Int. Conf. System Sci.*, 2017, pp. 3123–3129.
[25] M. Nick, O. Alizadeh-Mousavi, R. Cherkaoui, and M. Paolone, "Security constrained unit commitment with dynamic thermal line rating," *IEEE Trans. Power Syst.*, vol. 31, no. 3, pp. 2014–2025, May 2016.
[26] M. E. Baran and F. F. Wu, "Network reconfiguration in distribution systems for loss reduction and load balancing," *IEEE Trans. Power Del.*, vol. 4, no. 2, pp. 1401–1407, Apr. 1989.
[27] C. Wang and H. Z. Cheng, "Optimization of network configuration in large distribution systems using plant growth simulation algorithm," *IEEE Trans. Power Syst.*, vol. 23, no. 1, pp. 119–126, Feb. 2008.
[28] L. Economics, "Estimating the value of lost load-briefing paper prepared for the electric reliability council of texas," *Inc. London Economics*, Boston, 2013.
[29] D. I. Papaioannou, C. N. Papadimitriou, A. L. Dimeas, E. I. Zountouridou, G. C. Kiokes, and N. D. Hatziargyriou, "Optimization & sensitivity analysis of microgrids using HOMER software-a case study," *MedPower 2014*, 2014, pp. 1–7.
[30] PVwatts Calculator, National Renewable Energy Labratory (NREL), [Online] Available:http://pvwatts.nrel.gov.
[31] M. Nazemi, P. Dehghanian, M. Alhazmi, and Y. Darestani, "Resilience enhancement of electric power distribution grids against wildfires," in *Proc. IEEE Ind. Appl. Soc. Annu. Meeting*, 2021, pp. 1–7.

Mostafa Nazemi (Student Member) received the B.Sc. degree in electrical engineering from the K. N. Toosi University of Technology, Tehran, Iran, in 2015, and the M.Sc. degree in energy systems engineering from the Sharif University of Technology, Tehran, Iran, in 2017. He is currently working toward the Ph.D. degree in electrical engineering with the Department of Electrical and Computer Engineering, George Washington University, Washington, DC, USA.

His research interests include power system resilience, power system planning and operation, energy optimizations, and smart electricity grid applications.

Mr. Nazemi was the recipient of the 2018 Certificate of Excellence in Reviewing by the Editorial Board Committee of the Journal of Modern Power and Clean Energy for his contributions to the journal.

Payman Dehghanian (Senior Member, IEEE) received the B.Sc., M.Sc., and Ph.D. degrees in electrical engineering from the University of Tehran, Tehran, Iran, in 2009, the Sharif University of Technology, Tehran, Iran, in 2011, and the Texas A&M University, Texas, USA in 2017, respectively.

He is currently an Assistant Professor with the Department of Electrical and Computer Engineering, George Washington University, Washington, DC, USA. His research interests include power system protection and control, power system reliability and resiliency, asset management, and smart electricity grid applications.

Dr. Dehghanian is the recipient of the 2013 IEEE Iran Section Best M.Sc. Thesis Award in Electrical Engineering, the 2014 and 2015 IEEE Region 5 Outstanding Professional Achievement Awards, and the 2015 IEEE-HKN Outstanding Young Professional Award.

Mohannad Alhazmi (Student Member, IEEE) received the B.Sc. and M.Sc. degrees in electrical engineering from Umm Al-Qura University, Saudi Arabia, in 2013, and The George Washington University, Washington D.C., USA, in 2017, respectively. He is currently working toward the Ph.D. degree with the Department of Electrical and Computer Engineering, The George Washington University.

He is currently with the Electrical Engineering Department, College of Engineering, King Saud University, Riyadh, Saudi Arabia. His research interests include power system control, reliability and resiliency of power grids and critical infrastructure, cyber security and smart electricity grid applications.

Yousef Darestani received the B.Sc. degree in civil engineering from the University of Tehran, Tehran, Iran, in 2011, the M.Sc. degree in structural engineering from the Sharif University of Technology, Tehran, Iran in 2014, and the Ph.D. degree in civil engineering from the Ohio State University, Columbus, OH, USA, in August 2019.

He is currently a Research Assistant Professor with the Civil, Environmental, and Geospatial Engineering Department, Michigan Technological University. Prior to joining MTU, he spent a year as a Postdoctoral Researcher with the Civil, Environmental, and Geospatial Engineering Department, Rice University. His research focuses on risk, reliability, and resilience assessment and enhancement of infrastructure systems, machine learning techniques, and wind engineering.

Authorized licensed use limited to: The George Washington University. Downloaded on August 05,2022 at 03:56:01 UTC from IEEE Xplore. Restrictions apply.